Porcine Intestinal Enteroids: a New Model for Studying Enteric Coronavirus PEDV Infection and the Host Innate Response

Liang Li[1,*], Fang Fu[1,*], Shanshan Guo[1], Hongfeng Wang[2], Xijun He[1], Mei Xue[1], Lingdan Yin[1], Li Feng[1], Pinghuang Liu[1,#]

1. State Key Laboratory of Veterinary Biotechnology, Harbin Veterinary Research Institute, Chinese Academy of Agricultural Sciences; 2. Weike Biotechnology, Harbin Veterinary Research Institute, Chinese Academy of Agricultural Sciences, Harbin, China, 150069

Running title: Generation of swine enteroids for PEDV infection

 # To whom correspondence should be addressed:

Pinghuang Liu, Ph.D., E-mail: liupinghuang@caas.cn

*** These authors contributed equally to this work**

Abstract word count: 205

Text word count: 5252

Abstract

Porcine epidemic diarrhea virus (PEDV), a member of the group of alphacoronaviruses, is the pathogen of a highly contagious gastrointestinal swine disease. The elucidation of the events associated with the intestinal epithelial response to PEDV infection has been limited by the absence of good *in vitro* porcine intestinal models that recapitulate the multicellular complexity of the gastrointestinal tract. Here, we generated swine enteroids from the intestinal crypt stem cells of the duodenum, jejunum, or ileum, and found that the generated enteroids are able to satisfactorily recapitulate the complicated intestinal epithelium *in vivo* and are susceptible to infection by PEDV. PEDV infected multiple types of cells including enterocytes, stem cells, and goblet cells, and exhibited segmental infection discrepancies compared with ileal enteroids and colonoids, and this finding was verified *in vivo*. Moreover, the clinical isolate PEDV-JMS propagated better in ileal enteroids than the cell-adapted PEDV CV777, and PEDV infection suppressed IFN production early during the infection course. IFN-lambda elicited a potent antiviral response and inhibited PEDV in enteroids more efficiently than IFN-α. Therefore, swine enteroids provide a novel *in vitro* model for exploring the pathogenesis of PEDV and for the *in vitro* study of the interplay between a host and a variety of swine enteric viruses.

Keywords: porcine epidemic diarrhea virus (PEDV), coronavirus, enteroids, intestinal crypt cell, interferon

43 **Importance**

44 PEDV is a highly contagious enteric coronavirus that causes significant
45 economic losses, and the lack of a good *in vitro* model system is a major roadblock to
46 an in-depth understanding of PEDV pathogenesis. Here, we generated a porcine
47 intestinal enteroid model for PEDV infection. Utilizing porcine intestinal enteroids,
48 we demonstrated that PEDV infects multiple lineages of the intestinal epithelium and
49 preferably infects ileal enteroids over colonoids and that enteroids prefer to respond to
50 IFN-lambda 1 over IFN-α. These events recapitulate the events that occur *in vivo*.
51 This study constitutes the first use of a primary intestinal enteroid model to
52 investigate the susceptibility of porcine enteroids to PEDV and to determine the
53 antiviral response following infection. Our study provides important insights into the
54 events associated with PEDV infection of the porcine intestine and provides a
55 valuable *in vitro* model for studying not only PEDV but also other swine enteric
56 viruses.

57 **Introduction**

58 The complicated multicellular epithelial surfaces of the intestine contain the
59 primary sites of infection for many gastrointestinal (GI) pathogens and the interfaces
60 for interactions with microorganisms (1, 2). However, fundamental knowledge of the
61 intestinal epithelial cell-pathogen interactions in pigs is limited due to the lack of a
62 reliable *in vitro* model that recapitulates the complicated intestinal epithelium *in vivo*.
63 The intestinal epithelium is composed of villi and crypts, and the self-renewing and
64 undifferentiated stem cells in the crypt zone are responsible for the renewal of an
65 entire unit (3, 4). Unlike the classical *in vitro* models of transformed cancer cell lines,
66 enteroids derived from intestinal crypts contain a stem cell niche and diverse highly
67 polarized intestinal epithelial cell types (enterocytes, goblets, enteroendocrine, and
68 Paneth cells); thus, these enteroids well mimic the diverse cellular nature and
69 physiological activity of the intestine *in vivo* and represent a new *in vitro* model of the
70 infection of the intestinal epithelium by enteric pathogens (5-7). Intestinal enteroids
71 maintain the unique characteristics of the tissue from which they are derived and
72 recapitulate many of the biological and physiological properties of the small intestine
73 *in vivo* (4, 6, 8). As a result, since rodent and human intestinal enteroids were first
74 reported in 2009 and in 2010, respectively, intestinal enteroids have been applied in
75 enteric infection research and have yielded exciting new insights into a variety of
76 aspects of host-virus interactions in the GI tract (4, 7, 9-11). However, enteric
77 infection in porcine intestinal enteroids has not yet been reported.

78 Porcine epidemic diarrhea virus (PEDV), a member of the genus

alphacoronavirus in the family Coronaviridae, is the foremost causative agent of acute diarrhea, dehydration and high mortality in seronegative neonatal piglets, which result in substantial economic losses each year (12, 13). PEDV is highly enteropathogenic, primarily infects the villous epithelia of the small intestine, blunts the affected villi and disrupts the mucosal barrier integrity *in vivo* (14, 15). The identity of the specific cell types targeted (enterocytes, goblets, Paneth cells, microfold cells, tuft cells, or stem cells) by PEDV infection *in vivo* has remained elusive. However, most *in vitro* studies of PEDV have been performed in nonporcine cell lines such as Vero cells from an African green monkey kidney and HEK293 cells from a human embryonic kidney (16-18). Unlike normal mammalian cells, Vero cells are interferon-deficient cells that are incapable of producing type I interferons when infected by viruses (19). IPEC-J2 cells, a nontransformed porcine jejunum epithelial cell line from nonsuckling piglets (20), do not mimic the *in vivo* complicated epithelia, and PEDV clinical isolates generally do not replicate very well in porcine nontransformed epithelial cells such as IPEC-J2 (21, 22). The absence of a robust experimental *in vitro* system that can recapitulate the *in vivo* PEDV infection process is a bottleneck hampering the investigation of PEDV pathogenesis and the development of novel rational strategies against PEDV infection. Therefore, the development of *in vitro* models that can closely recapitulate the porcine intestine is crucial for expanding the current knowledge of PEDV pathogenesis and facilitating further biological investigations of host-PEDV interactions.

In the present study, we generated crypt cell-derived enteroids and used this

model to study PEDV infection. The results revealed that porcine enteroids were susceptible to PEDV infection and recapitulated many of the events associated with PEDV infection in porcine intestines *in vivo*. Collectively, these data illustrate that porcine enteroids, which recapitulate the key properties of the *in vivo* intestinal epithelium, provide an invaluable resource for addressing fundamental aspects of enteric coronaviruses that cannot be modeled using traditional cell lines.

Results

Generation of porcine intestinal enteroids derived from intestinal crypt stem cells

To closely mimic the events associated with enteric virus infection in the swine intestine, we generated primary porcine enteroid cultures derived from piglet intestinal crypts containing leucine-rich repeat-containing G-protein-coupled receptor 5 (Lgr5)-positive stem cells. Crypts from the duodenum, jejunum, or ileum were freshly isolated as described previously with slight modification and were cultured in a semisolid, laminin/collagen-rich Matrigel in proliferation medium to allow their differentiation into three-dimensional (3D) enteroids in 7 to 15 days using previously developed methods (4, 11, 23). After a period of approximately 1 to 2 weeks in Matrigel culture, the intestinal crypt cells proliferated and differentiated into 3D enteroids with a central lumen surrounded by an epithelium containing villus-like structures and budding crypt-like domains, which indicated that the crypt cells from all three small intestine regions could grow into enteroids (Fig. 1A). Because most of

123 the reported enteroid studies have been performed using ileal enteroids, we used ileal
124 enteroids as representative intestinal enteroids and performed most of the experiments
125 of the current study using ileal enteroids. To evaluate whether the differentiated
126 enteroids could be cryopreserved and thawed and whether the resulting thawed cells
127 could differentiate into enteroids, as previously reported, differentiated ileal enteroids
128 were subjected to a freeze-thaw cycle and then differentiated as if they were freshly
129 isolated crypt stem cells. The thawed ileal enteroid single cells grew into enteroids in
130 7 days (Fig. 1B), and thus, we developed a porcine crypt-derived 3D enteroid culture
131 system.

132 Because the apical membrane of the 3D enteroids for viral infection faces the
133 inside of the enteroids, the infection of 3D enteroids is challenging. We thus sought to
134 develop a porcine planar (2D) ileal enteroid culture in microplates, which would make
135 them amenable for efficient infection and would allow deciphering of the complex
136 interplay between viruses and epithelial cells. Previous studies demonstrated that
137 dissociated 3D mouse enteroids can generate planar enteroid monolayers with proper
138 apical and basal polarity that largely recapitulate the many features of 3D enteroids
139 and the *in vivo* intestinal epithelium (23, 24). The 3D ileal enteroids that were
140 expanded in Matrigel were harvested, mechanically dissociated and seeded on
141 Matrigel-coated microplates to establish 2D enteroids as described previously (24).
142 After expansion and differentiation, the seeded cells grew out as large, contiguous
143 sheets of epithelium with heterogeneity in terms of cell morphology and densities (Fig.
144 1C). A large number of villin-positive enterocytes were present on the apical surface

and throughout the 2D monolayer (Fig. 1D), indicating the presence of mature enterocytes in the enteroids. Proliferating cells stained with Ki-67 protein and stem cells (Lgr5+) were present throughout the 2D monolayers, which suggested that our 2D enteroids maintain the features of stem cells and contain the transit-amplifying zone. We also identified Paneth (lysozyme-C (LYZ)+) cells, goblet (mucin2 (Muc2)+) cells, and enteroendocrine (chromogranin A (CHGA)+) cells in the 2D ileal enteroids (Fig. 1D). Thus, the planar intestinal enteroids generated from budding crypt-like 3D enteroids include multiple cell lineages and recapitulate the varied cellular phenotypes of the intestinal epithelium. Moreover, a lumen-like structure was identified in the differentiated planar 2D ileal enteroids (Fig. 1D). Altogether, these results demonstrate that a planar swine enteroid culture can be generated from intestinal crypt stem cells.

Porcine intestinal enteroids are susceptible to PEDV infection

To determine whether porcine intestinal enteroids are permissible to infection by PEDV, we inoculated porcine ileal enteroids with the clinical isolate PEDV-JMS at increasing multiplicities of infection (MOIs). At 48 h postinfection (hpi), the numbers of PEDV genomes were substantially increased from 34- to 754-fold greater than their levels at 2 hpi and were correlated with the MOI (Fig. 2A), indicating that PEDV can infect enteroids. It is well established that PEDV primarily infects the small intestine and can infect all three regions (duodenum, jejunum, and ileum) of the small intestine. To assess the potential existence of a disparity in the susceptibility to PEDV infection among duodenal, jejunal, and ileal enteroids, we infected the three enteroids with the

same MOI and monitored the viral replication kinetics. The duodenal, jejunal, and ileal enteroids were all infected by PEDV, and the results showed that PEDV genomes had increased up to 63-fold at 24 hpi compared with 2 hpi and peaked at 48 hpi, indicating successful PEDV replication in all three enteroids. In addition, the enteroids derived from duodenum, jejunum, and ileum exhibited similar viral replication kinetic levels after PEDV infection (Fig. 2B). PEDV infection in ileal enteroids was further confirmed through an anti-PEDV nucleocapsid immunofluorescence assay (IFA) (Fig. 2C). Successful PEDV infection in ileal enteroids resulted in a significant cytopathic effect and disruption of the enteroid structure starting at 24 hpi, and this structure continued to deteriorate over time (Fig. 2D). These results indicate that PEDV successfully infects enteroids and establishes a productive infection.

Because intestinal enteroids contain multiple cell-type compositions, we then took advantage of the multiple cellular phenotypes of intestinal enteroids and sought to clarify whether PEDV targets specific cell types in the porcine intestinal enteroids through double immunofluorescent labeling (Fig. 3A). We detected PEDV infection in differentiated mature enterocyte cells that express villin, which serves as a surface marker for differentiated intestinal epithelial cells and is expressed in cells located in the brush border of the intestine (25, 26). Moreover, we observed PEDV infection (nucleocapsid-positive) in Lgr5+ stem cells, Ki-67-positive (proliferating) cells, and Muc2+ goblet cells, although the number of PEDV-positive cells in the latter two cell populations was limited (Fig. 3A). These results indicate that PEDV infects multiple

189 cell lineages, including stem cells and goblet cells. Thus, these data show that PEDV
190 can infect enteroids, including enterocytes, stem cells, and goblet cells.

191 To further verify whether PEDV infects multiple cell lineages *in vivo*, we
192 subjected ileal tissues collected from PEDV-infected piglets to immunohistochemistry
193 staining. Consistent with previous reports, PEDV infection caused severe atrophic
194 enteritis, and PEDV antigen-positive cells were largely located along the sides of villi,
195 suggesting that PEDV successfully infects ileal tissue (Fig. 3B) (27). We also
196 performed double immunofluorescent staining of the same sample with anti-PEDV
197 spike protein and anti-cell markers (villin, Lgr5, Ki-67, and Muc2) (Fig. 3C). As
198 expected, villin, a marker of mature enterocytes, was present along the apical side of
199 the intestinal villus, and PEDV infection was distributed throughout the villin+ villi.
200 PEDV infection was primarily located on the tip and waist of villi, and Lgr5-positive
201 cells were primarily concentrated at the bottom crypt area of intestinal villi. We easily
202 identified significant PEDV infection in Lgr5+ cells in the crypt area (Fig. 3C), which
203 indicates that PEDV infects Lgr5+ crypt stem cells, as observed *in vitro* in enteroids.
204 Unlike Lgr5 staining, which was concentrated in the bottom crypt, Ki-67-positive
205 cells were distributed widely in the proliferative zone of the crypt and reached the
206 waist area of villi (Fig. 3C). PEDV protein was occasionally observed in Ki-67+
207 proliferating epithelial cells and to a lesser degree in Muc2+ goblet cells (Fig. 3C).
208 These results demonstrate that PEDV is capable of infecting multiple cellular lineages,
209 including enterocytes, stem cells, and goblet cells, as observed *in vitro*. Thus,
210 intestinal enteroids provide a unique platform for studying the multiple cellular targets

of PEDV and the effect of PEDV infection on these various epithelial lineages.

PEDV preferentially infects ileal enteroids compared with colonoids

PEDV largely infects the villous epithelial cells of the small intestine *in vivo*, although restricted infection has also been observed in the colon (15). To recapitulate the segmental discrepancy of PEDV infection observed *in vivo*, we isolated crypt stem cells from ileal and colonic tissues from the same piglet. The stem cells from both ileal and colonic crypts expanded and differentiated into enteroids and colonoids, respectively (Fig. 1A and 4A), but the rates of intestinal organoid differentiation were not identical. Approximately 7 days were required for the ileal crypt stem cells to differentiate into enteroids, whereas the colonic crypt stem cells required a longer time (approximately two weeks) to differentiate into colonoids (Fig. 4A). Consistent with the segmental discrepancy of PEDV infection observed *in vivo* in the intestine, PEDV infected both ileal enteroids and colonoids but showed restricted infection in colonoids (Fig. 4B). The number of PEDV genome copies in colonoids at 72 hpi was increased only approximately 5-fold compared with that at 2 hpi, whereas the number of PEDV genome copies in ileal enteroids was substantially elevated from 24 to 72 hpi to reach values at 72 h that were 1527-fold higher than those at 2 hpi. Consistent with the PEDV genome numbers, 24 to 72 hpi at the same MOIs, ileal enteroids produced up to 44-fold more infectious particles than colonic enteroids (Fig. 4C). The discrepancy in infection between ileal enteroids and colonoids was further confirmed by PEDV N protein IFA (Fig. 4D), and the results were consistent with the *in vivo* results: PEDV infection did not cause prominent pathological injury to colonic villi,

and only a limited number of PEDV antigen-positive cells were detected in the colonic villi (Fig. 4E). Our results suggest that enteroids retain the internal region-specific identity among intestine segments. These data demonstrate that enteroid systems well mimic the events that occur during PEDV infection *in vivo*.

Clinical PEDV isolate showed better propagation in ileal enteroids than the cell-adapted strain CV777

The growth of clinical isolates of PEDV in cell lineages such as Vero E6 cells is typically challenging. Often, cell-adapted PEDV grows well in continuous cell lines, such as Vero E6 cells, after being subjected to multiple rounds of blind passaging in the cell line. We subsequently compared the replication of the clinical isolate PEDV-JMS in porcine ileal enteroids with that of the cell-adapted PEDV CV777. After infection at the equivalent MOI, PEDV-JMS in ileal enteroids produced up to 473-fold higher levels of viral genomes than those obtained with PEDV CV777 throughout the study period (Fig. 5A). Consistent with the RNA results, PEDV-JMS produced more viral titers in enteroids, yielding values that were 49- to 140-fold than those obtained with PEDV-CV777 (Fig. 5B), which indicated that the clinical isolate PEDV-JMS exhibits better infection in ileal enteroids than the cell-adapted strain CV777. PEDV N protein IFA further confirmed that PEDV-JMS propagated better in enteroids than PEDV CV777, even though both viruses infected enteroids (Fig. 5C). These data indicate that enteroids can be a good culture system for isolating clinical PEDV isolates.

PEDV infection suppresses the induction of innate IFN responses in enteroids

255 Recent studies have shown that PEDV infection inhibits the production of type I
256 and III IFN in IEC cell lines such as IPEC-J2 (21). To verify whether PEDV infection
257 inhibits the innate IFN responses in enteroids, we monitored the mRNA transcripts of
258 type I IFN (IFN-α) and type III IFN-lambda 1 (IFN-L1) by RT-qPCR in enteroids at
259 various time points after infection with PEDV-JMS. Compared with the mock
260 uninfected control, PEDV-JMS caused a rapid and substantial reduction in the
261 expression of IFN-α and IFN-L1 transcripts, as observed at 2 and 12 hpi, and this
262 decrease was followed by the induction of IFN expression after 24 hpi, indicating that
263 PEDV infection inhibits the induction of type I and III IFN at the early stage of
264 infection. However, the IFN-α and IFN-L1 expression kinetics were not identical (Fig.
265 6A and 6B): IFN-α peaked at 24 hpi, whereas IFN-L1 peaked at 48 hpi. To further
266 verify that PEDV infection suppresses the induction of IFNs, we assessed IFN-L1
267 production after stimulating PEDV-infected enteroids at 12 hpi with poly(I:C) for 12
268 h. Stimulation with poly(I:C) substantially increased the expression of IFN-L1 in
269 enteroids (Fig. 6C), which suggested that enteroids are capable of efficiently
270 producing IFN-L1. In contrast, PEDV infection for 12 hpi significantly reduced the
271 poly(I:C)-elicited production of IFN-L1 (Fig. 6C), which suggested that PEDV
272 suppresses IFN production in enteroids. These findings indicate that intestinal
273 enteroids are a suitable *ex vivo* model for the study of innate immunity in response to
274 PEDV infection.

275 **IFN-L1 induces potent ISG expression and inhibits PEDV infection in ileal**
276 **enteroids**

277 We and others have shown that compared with IFN-α, IFN-L1 selectively acts
278 on IPEC-J2 cells and induces potent interferon-stimulated gene (ISG) expression (21,
279 28). To gauge the antiviral activities of type III and I IFNs against virus infection in
280 enteroids, we initially monitored ISG expression in enteroids that had been primed for
281 24 h with either IFN-L1 or IFN-α. Both IFN-L1 and IFN-α elicited potent expression
282 of interferon-stimulated gene 15 (ISG15) (Fig. 7A), MxA (Fig. 7B),
283 2'-5'-oligoadenylate synthetase-like protein (OASL) (Fig. 7C), and interferon-induced
284 transmembrane protein 1 (IFITM1) (Fig. 7D) in a dose-dependent manner after
285 stimulation. Consistent with the previous results in IPEC-J2 cells, IFN-L1 induced
286 significantly higher levels of ISG15, OASL, MxA, and IFITM1 in enteroids than
287 IFN-α, regardless of the concentrations of IFNs (Fig. 7A-7D). In agreement with the
288 ISG expression profiles elicited by IFN-L1 and IFN-α, both IFN-L1 and IFN-α
289 inhibited PEDV infection in enteroids in a dose-dependent manner, although IFN-L1
290 showed stronger antiviral activity against PEDV than IFN-α (Fig. 7E and 7F). These
291 results demonstrate that IFN-L1 exhibits increased activity on enteroids than IFN-α.
292 In summary, intestinal enteroids present a good *in vitro* model for evaluating the
293 innate response to PEDV infection.

294

295 **Discussion**

296 PEDV is primarily transmitted through the fecal-oral route and infects intestinal
297 villous epithelial cells *in vivo* (12, 27). The current *in vitro* cell cultures of PEDV
298 include Vero cells (29), MARC-145 cells (another monkey kidney cell line), HEK293

299 cells (30), and IPEC-J2 cells (21, 31), and most of these are nonporcine intestinal
300 epithelial cells and thus not the ideal *in vitro* cellular models for studying the
301 interaction between PEDV infection and the host response due to interspecific
302 variation. Although IPEC-J2 cells are a nontransformed porcine intestinal epithelial
303 cell line, these cells lack the complexity of the cell types found in and the architecture
304 of the intestinal epithelium and thus do not satisfactorily mimic the natural infection
305 process. Intestinal enteroids represent a significant advantage over traditional *in vitro*
306 models and provide a unique opportunity to explore host-pathogen interactions in an
307 *in vitro* system that recapitulates the complicated cellularity of the GI tract. Although
308 great progress has been achieved in generating human and mouse intestinal enteroids
309 and using *ex vivo* systems to better understand the intestinal physiology and
310 pathophysiology of enteric infection, previous studies have not investigated enteric
311 viral infection in enteroids derived from porcine crypt stem cells. Here, we established
312 a porcine enteroid culture system from crypt cells that contains enterocytes,
313 enteroendocrine cells, goblet cells, Paneth cells, and stem cells and found that the
314 proposed system well recapitulates the complex intestinal epithelium *in vivo* (Fig. 1).
315 The porcine crypt enteroids derived from all three small intestinal regions were found
316 to be permissible to infection by PEDV and provide a unique platform for studying
317 intestinal physiology and a variety of biological aspects of porcine enteric pathogens.

318 The use of enteroids represents a significant advantage over traditional *in vitro*
319 methods because they closely mimic the structure and function of the small intestine
320 while maintaining the genetic identity of the host. Enteroids derived from crypt stem

cells from different intestinal segments of the same donor allow assessment of the contribution of different intestinal segments to PEDV infection. Previous studies and our results have shown that PEDV largely infects the epithelial cells of the small intestine and occasionally infects colon epithelial cells (Figs. 2, 3 and 4) (27, 32). In fact, we observed differential susceptibilities to PEDV infection between colonoids and ileal enteroids (Fig. 4B-4D), indicating that the segment-specific difference is maintained *ex vivo* in enteroid cultures. These data illustrate the utility of the enteroid system for addressing fundamental aspects of PEDV that cannot be modeled using standard cell lines.

Due to their unique features, enteroids better mimic the multiple cell types of the intestinal epithelium *in vivo* than traditional cell line models. We observed that PEDV was capable of infecting goblet cells and stem cells in addition to the primary cellular target, villous mature enterocytes, in the enteroids, and this finding was confirmed *in vivo* in the PEDV-infected ileum (Fig. 3C). The intestinal epithelium is a rapidly self-renewing tissue, and the turnover rate for complete renewal is approximately 3–5 days (33). The Lgr5+ stem cells in crypts are primarily responsible for replenishing the high turnover of the intestinal epithelium. PEDV infection is cytolytic and causes acute necrosis of the infected enterocytes, leading to marked intestinal villous atrophy (12, 14, 15). Elucidating the effect of PEDV infection on crypt proliferation and differentiation has been a critical challenge. Only two previous reports have shown that PEDV infection causes a substantial increase in Ki-67-positive cells and induces the localization of large numbers of Lgr5+ cells in the crypt niches of the intestine of

343 PEDV-infected pigs (13, 15). A previous study conducted by Jung et al. showed that
344 the numbers of Lgr5+ cells and the proliferation of crypt cells are associated with
345 piglet age, which is associated with susceptibility to PEDV infection (13). These
346 results indicate that crypt stem cells are involved in the pathogenesis of PEDV
347 infection. However, whether PEDV directly infects Lgr5+ stem cells is unknown.
348 Madson et al. previously visualized PEDV protein at the villus-crypt interface of the
349 distal jejunum and ileum early during the infection process (32). Here, we directly
350 observed PEDV proteins in Lgr5+ cells and Ki-67+ transit-amplifying cells in both
351 ileal enteroids and infected ileal tissue. Enterocytes move forward luminal surfaces
352 from the bottom crypt area as they differentiate and mature, but further studies are
353 needed to clarify whether the location and maturity of enterocytes influence the
354 susceptibility of PEDV infection in these cells. In contrast to the previous *in vivo*
355 study (27), we did not observe a significant increase in Ki-67+ epithelial cells
356 following PEDV infection in enteroids. Other factors might be involved in the
357 increase in Ki-67+ epithelial cells during *in vivo* PEDV infection, and enteroids
358 provide a good *in vitro* model to further address this question.

359 Goblet cells are simple columnar epithelial cells that constitute the primary
360 cellular source of Muc2 mucins (34, 35). Mucins form an intestinal inner mucus layer,
361 which serves as a physical barrier that effectively separates the commensal microbiota
362 from the single epithelial cell layer and plays crucial roles in the maintenance of
363 microbial homeostasis and the protection of epithelial cells from infection (36, 37).
364 Jung et al. previously detected a PEDV antigen in goblet cells and demonstrated that

365 PEDV infection caused a substantial reduction in goblet cells in the small intestine
366 (27, 38). In agreement with the previous *in vivo* results, we observed that PEDV
367 infected goblet cells of enteroids *in vitro*. Another porcine alphacoronavirus,
368 transmissible gastroenteritis virus (TGEV), reportedly binds to mucin on the apical
369 membrane of intestinal cells, which allows TGEV to stay longer in the intestine and
370 facilitates intestinal infection (39). However, whether PEDV takes advantage of
371 mucin to facilitate the infection of goblet cells and the effect of PEDV infection on
372 the functions of goblet cells remain unclear. In addition to the secretion of mucins,
373 goblet cells play crucial roles in the presentation of oral antigens to the immune
374 system (34). In the future, it will be very interesting to further explore the effect of
375 PEDV infection on the functions of goblet cells by taking advantage of the enteroid
376 model.

377 In summary, we show that porcine enteroids can be used to model the
378 multicellular phenotype of the intestinal epithelium, which serves as the primary
379 portal through which enteric viruses enter the hosts. Our findings provide important
380 insights into events associated with PEDV infection and demonstrate that swine
381 enteroids can be used as a unique model to define the complicated crosstalk that exists
382 between PEDV and the intestinal epithelium, which would undoubtedly have
383 profound impacts on the clarification of PEDV pathogenesis. Intestinal enteroids also
384 provide a platform for exploring the role of additional host factors in cellular tropism
385 and can be used to isolate and grow previously uncultivable enteric viruses.
386

387 **Materials and Methods**

388 **Cell cultures.** African green monkey kidney cells (Vero E6) were grown and
389 maintained in Modified Eagle's Medium (DMEM) supplemented with antibiotics (100
390 units/mL penicillin and 100 μg/mL streptomycin) and 10% heat-inactivated fetal
391 bovine serum (FBS) (Gibco).

392 **Virus stocks, titration, and infection of cells**. The Vero cell-adapted PEDV CV777
393 strain (GenBank Accession No KT323979) was propagated as previously described
394 (40, 41). The PEDV-JMS strain (passage 6) was isolated and stocked by our
395 laboratory, and the PEDV stock was prepared and titrated as described previously (22,
396 40). To assess the anti-PEDV activity of IFN-α and IFN-L1, cells were infected with
397 PEDV after being primed with the indicated concentrations of IFN for 24 h. Samples
398 were collected at the indicated times postinfection for the quantification of PEDV
399 infection.

400 **Porcine intestinal crypt isolation and 3D enteroid culture.** Porcine intestinal crypts
401 were prepared from specific pathogen-free 2-10-day-old piglets using previously
402 described protocols with minor modifications (11, 23). Briefly, the intestine was
403 opened lengthwise and cut into 2-mm segments. The intestinal pieces were washed
404 several times until the supernatant was clear, and the washed intestinal pieces were
405 hen suspended in Gentle Cell Dissociation Reagent (STEMCELL, Canada) to
406 disassociate the crypts. The pellets of the intestinal pieces were suspended in 10 mL
407 of cold PBS with 0.1% bovine serum albumin (BSA) and antibiotics pen-strep and
408 passed through a 70-μm filter. The crypt pellets were harvested by centrifugation at

409 200×g and 4 °C for 5 min and resuspended in 10 mL of cold DMEM/F-12. After
410 counting, the intestinal crypts were resuspended with IntestiCult Organoid Growth
411 Medium (STEMCELL, Canada) and Matrigel (BD Biosciences, USA) and seeded
412 into a 48-well plate at a density of 50 crypts per well. The plate was incubated at
413 37 °C for 10 min until the Matrigel solidified, and 300 μL of IntestiCult Organoid
414 Growth Medium was then added to each well. The plate was subsequently incubated
415 at 37 °C in a 5% CO_2 incubator, and the culture medium was exchanged every 3-4
416 days. The Institutional Animal Care and Use Committee of the Harbin Veterinary
417 Research Institute approved all the protocols used for animal experiments in this
418 study.

419 **2D monolayer enteroid culture.** Expanded 3D enteroids were recovered from
420 Matrigel after 7-14 days of growth through the addition of ice-cold DMEM/F-12
421 medium, transferred into 15-mL tubes, and centrifuged at 250 ×g and 4 °C for 5 min.
422 The enteroid pellet was incubated in 0.25% Trypsin-EDTA 1X (Gibco) for 5 min at
423 37 °C and dissociated by repeated pipetting to obtain a single-cell suspension.
424 DMEM/F-12 with 10% (v/v) FBS was added to the single-cell suspension, and the
425 mixture was centrifuged at 800 ×g for 5 min. The cell pellets were resuspended in
426 complete IntestiCult Organoid Growth Medium at room temperature and seeded at 50
427 enteroid cells per well in a Matrigel-precoated 96-well plate. After 3 days of
428 differentiation, the planner monolayer 2D enteroids were ready for experiments.

429 **Experimental infection of piglets.** Four 10-day-old specific pathogen-free (SPF)
430 piglets were randomly divided into two groups. The SPF piglets in group one were

orally inoculated with 1.0 mL of 4.5×10^5 $TCID_{50}$ PEDV-JMS strain, and the SPF piglets in group two were inoculated with 1.0 mL of DMEM and served as uninfected controls. All clinical signs were recorded on a daily basis after virus infection, and all the piglets were euthanized at 4 days postinfection. The Animal Ethics Committee approved the protocol under the following approval number: Heilongjiang-SYXK-2006-032. Intestinal samples from the piglets were collected for pathological evaluation and assessment of PEDV infection.

RNA isolation and reverse transcriptase quantitative PCR (RT-qPCR). Total cellular mRNA was extracted using the Simply P Total RNA Extraction Kit (BioFlux, China) according to the manufacturer's instructions. Total mRNA (1 μg) was reverse transcribed to cDNA using the PrimeScript™ II 1st Strand cDNA Synthesis Kit (Takara, China), and relative gene expression levels were quantified by qPCR using SYBR green PCR mix (Life Technologies, USA) based on the cycle threshold ($\Delta\Delta C_T$) method (42). GAPDH served as the internal control. The primers were designed using Primer Premier 5 software and are listed in Table 1.

Hematoxylin and eosin (H&E) staining. Formalin-fixed ileum sections were serially dehydrated with 70%, 95%, and 100% ethanol, cleared in xylene, embedded in paraffin wax, and sectioned at 4–6-μm thickness. After dewaxing in xylene and serially rehydrating with 100%, 95%, and 70% ethanol, the ileum sections were stained with hematoxylin and eosin (HE; Sigma-Aldrich) for histopathological evaluation and observed using a light microscope.

Immunohistochemistry. Ileum or colon tissue sections were deparaffinized in xylene

453 and rehydrated with water containing descending concentrations (100%, 95%, and
454 70%) of ethanol. The slide was immersed in a citric acid (pH 7.4)/sodium citrate
455 buffer solution (pH 8.0) at 121 °C for 30 min for antigen retrieval. The tissues were
456 rinsed with running tap water for 5 min and phosphate-buffered saline (PBS; Gibco)
457 for 5 min, immersed in 3% (v/v) H_2O_2-methanol solution for 30 min to block
458 endogenous peroxidase activity, rinsed with running tap water for 5 min, and then
459 blocked with 5% skim milk (Sigma-Aldrich, USA) in PBS for 30 min at room
460 temperature. Mouse anti-PEDV spike protein monoclonal antibody (mAb) 6E5
461 (stocked in our laboratory) was diluted 1:200 in PBS. After overnight incubation at
462 4 °C, the tissue sections were subjected to three 10-min washes with PBS.
463 Subsequently, the slides were incubated with goat anti-rabbit secondary antibody in
464 the dark for 30 min at room temperature, subjected to three 5-min washes with PBS,
465 visualized rapidly using diaminobenzidine (DAB) (Sigma-Aldrich, USA), and
466 counterstained with hematoxylin. The slides were then dehydrated with ascending
467 concentrations (70%, 95%, and 100%) of ethanol, clarified in xylene, and mounted
468 with Entellan mounting medium (Sigma-Aldrich, USA). The staining was observed
469 using an optical microscope.

470 **Immunofluorescence assay (IFA).** Porcine intestinal enteroids (PIE) monolayers
471 were infected with PEDV-JMS at an MOI of 5. The level of PEDV infection at 48 h
472 postinfection and the expression of differentiation markers were analyzed by IFA as
473 described previously (22). Briefly, PIE monolayers were fixed with 4%
474 paraformaldehyde (PFA) for 30 min at room temperature (RT). After permeabilization

475 with 0.2% Triton X-100, the cells were blocked with blocking buffer (PBS with 5%
476 FBS and 5% skim milk), incubated with the primary antibodies for 2 h at 37 °C, and
477 stained with the secondary antibodies for 1 h at 37 °C. The surface differentiation
478 markers of intestinal epithelial cells were detected using primary anti-Ki-67 (1 μg/mL,
479 Abcam, USA) for proliferative cells, anti-Lgr5 (1:50, Novus Biologicals, USA) for
480 stem cells, anti-mucin 2 (1:50, Abcam, USA) for goblet cells, anti-villin (1:100,
481 Abcam, USA) and anti-chromogranin A (1:100, Santa Cruz, USA) for
482 enteroendocrine and anti-lysozyme (1:50, Santa Cruz, USA) for Paneth cells. Mouse
483 anti-PEDV nucleocapsid monoclonal antibody (mAb) 2G3 was stocked in our
484 laboratory (1:180 dilution). The cells were then labeled with secondary antibody
485 conjugated to Alexa Fluor 488 donkey polyclonal antibody against rabbit IgG (1:1000,
486 Thermo Fisher Scientific, USA) or Alexa Fluor 546 goat anti-mouse IgG antibody
487 (1:500, Thermo Fisher Scientific, USA). DAPI (1:100, Sigma, USA) was used to stain
488 cellular nuclei. The stained cells were visualized using an EVOS FL Auto2
489 fluorescence microscope.

490 Representative sections of ileum or colon tissues were deparaffinized, rehydrated,
491 heated for antigen retrieval, and blocked with 5% skimmed milk. Mouse anti-PEDV
492 spike protein mAb 6E5 (1:200 dilution) was stocked in our laboratory. The surface
493 differentiation markers of intestinal epithelial cells were stained as described above.
494 The tissue sections were then rapidly washed three times in PBS, incubated with
495 DAPI for 10 min at room temperature, and mounted. The slides were imaged using a
496 Carl Zeiss microscope (LSM700, Carl Zeiss, Heidenheim, Germany) with the

appropriate filter set.

Statistical analysis. All the results in the figures are presented, wherever appropriate, as the means ± the standard errors of the mean (SEMs) from three independent experiments and were analyzed using GraphPad Prism (GraphPad Software, Inc.). Differences were considered significant if the *P* value was <0.05. The *P* values are indicated as follows: **P* <0.05, ***P* <0.01, ****P* <0.005, and *****P* <0.001.

Acknowledgments

This work was supported by grants from the National Key R & D Program of China (2017YFD0502200) and the National Natural Science Fund (31772718).

509 **Table 1. Primers for qPCR**

Gene name		Primer sequence (5'-3')
MxA	Forward	CACTGCTTTGATACAAGGAGAGG
	Reverse	GCACTCCATCTGCAGAACTCAT
ISG15	Forward	AGCATGGTCCTGTTGATGGTG
	Reverse	CAGAAATGGTCAGCTTGCACG
OASL	Forward	TCCCTGGGAAGAATGTGCAG
	Reverse	CCCTGGCAAGAGCATAGTGT
IFITM1	Forward	TGCCTCCACCGCCAAGT
	Reverse	GTGGCTCCGATGGTCAGAAT
IFN-α	Forward	CTGCTGCCTGGAATGAGAGCC
	Reverse	TGACACAGGCTTCCAGGTCCC
IFN-L1	Forward	CCACGTCGAACTTCAGGCTT
	Reverse	ATGTGCAAGTCTCCACTGGT
PEDV	Forward	GCACTTATTGGCAGGCTTTGT
CV777 ORF3	Reverse	CCATTGAGAAAAGAAAGTGTCGTAG
PEDV-JMS ORF3	Forward	CACTTATTGGCAGGCTCTTT
	Reverse	CCATTGAGAAAAGAAAGTGTAGTAG
GAPDH	Forward	CCTTCCGTGTCCCTACTGCCAAC
	Reverse	GACGCCTGCTTCACCACCTTCT

510

511

512 **Figure legends**

513 **Fig. 1. Generation of porcine enteroids derived from intestinal crypt stem cells.**
514 (A). Representative images of the time course of porcine enteroid differentiation from
515 intestinal crypts. During culture in Matrigel, small spheroids formed on day 3 after
516 crypt isolation, gradually matured over time and formed budding-like crypt structures
517 on day 7. (B). Development of ileal enteroids from frozen-thawed enteroid cells.
518 Enteroids from frozen-thawed enteroid cells were cultured and differentiated as
519 described in panel A. (C). Representative images of the time course of ileal enteroid
520 monolayers differentiated from enteroid cell plating. Crypt-derived 3D enteroids were
521 enzymatically dissociated into single cells and seeded on precoated 96-well plates in
522 IntestiCult Organoid Growth Medium to differentiate for 3 days. (D). Identification of
523 different cell lineages in enteroid monolayers. Enteroid monolayer cultures were fixed
524 and costained for specific cell lineages in the porcine intestine using DAPI (nuclear
525 staining, blue) and surface marker antibodies: Lgr5 for stem cells (red), Ki-67 for
526 proliferating cells (red), villin for enterocytes (red), lysozyme-C (LYZ) for Paneth
527 cells (red), mucin2 (Muc) for goblet cells (red), and chromogranin A (CHGA) for
528 enteroendocrine cells (red) (bar = 200 μm).

529 **Fig. 2. Detection of PEDV infection in porcine planar enteroids.** (A). Detection of
530 PEDV infection in planar ileal enteroids by RT-qPCR. Monolayers of porcine ileal
531 enteroids were mock-inoculated or inoculated with PEDV-JMS at the indicated MOIs
532 for 2 h at 37 °C. The inoculated enteroids were washed three times with PBS and
533 harvested at 2 or 48 h postinfection. Total cellular RNA was extracted, and the

number of PEDV genome copies was determined by RT-qPCR. The data are presented as the means of three wells for each treatment and time point. The error bars denote the standard error deviations. (B). The kinetic curve of PEDV replication in enteroids derived from duodenal, jejunal, or ileal crypts. Monolayer enteroids were inoculated with PEDV at an MOI of 5, and the level of PEDV infection at different time points postinfection was quantified by RT-qPCR. (C). Detection of PEDV infection in enteroids by PEDV N protein IFA. Forty-eight hours after infection with PEDV at an MOI of 5, the enteroids were fixed with 4% paraformaldehyde, and the expression of PEDV N protein was detected with mouse anti-PEDV N mAb (red). DAPI was used to stain cellular nuclei (blue). (D). Brightfield images at various hours after PEDV-JMS infection (MOI=5).

Fig. 3. Identification of the cell phenotypes infected by PEDV *in vitro* and *in vivo*. (A). Double immunofluorescent labeling of ileal enteroids infected with PEDV-JMS at 48 hpi. Villin, Lgr5, Ki-67, and mucin2 were used as enterocyte, intestinal stem cell, proliferating cell, and goblet cell markers (green), respectively. PEDV was labeled with anti-PEDV N protein antibody (red). DAPI was used for nuclear staining. Scale bar = 100 μm. (B). *In vivo* H&E staining and immunohistochemistry assay with an antibody to PEDV S protein. Samples (ileum) were collected from SPF piglets inoculated orally with mock DMEM or PEDV-JMS (black arrows). Scale bar = 200 μm. (C). I*n vivo* double-labeling histoimmunofluorescence assay with antibodies, as described in A. Samples (ileum) were collected from SPF piglets inoculated orally with PEDV. Specific cell marker (green) and PEDV S (red) double-labeling cells are

indicated by light blue arrows. DAPI (blue) was used for nuclear staining. Scale bar = 50 μm.

Fig. 4. PEDV preferably infects ileal enteroids compared with colonoids. (A). Representative images of the time course of porcine colonoid development. Colonic crypts were isolated and differentiated into colonoids using the process used for the differentiation of ileal enteroids described in Fig. 1A. (B and C). Kinetic curve of PEDV-JMS replication in ileal enteroids or colonoids. Planar ileal enteroids or colonoids derived from the same piglet were infected with PEDV-JMS at an MOI of 5. The kinetics of PEDV production were determined by RT-qPCR (B) or titration (C). The data are presented as the means ± SEMs of three wells for each treatment and represent the results obtained for enteroids from two SPF piglets. The *P* values indicate the significance of the difference between ileal enteroids and colonoids. (D). Detection of PEDV infection in ileal enteroids or colonoids by IFA. Planner ileal enteroids or colonoids were infected with PEDV at an MOI of 5, and the level of PEDV infection at 48 hpi was detected by staining with anti-PEDV N mAb. Representative IFA images were randomly selected from four fields per well, and the PEDV+ cells were counted. The results are presented in the right bar graph. (E). *In vivo* H&E staining and immunohistochemistry assay with an antibody to PEDV S protein. Samples (colon) were collected from SPF piglets inoculated orally with mock DMEM or PEDV-JMS. Scale bar = 200 μm.

Fig. 5. PEDV-JMS exhibited better infection in ileal enteroids than PEDV CV777. (A and B). Viral replication kinetics of PEDV-JMS or CV777 in ileal enteroids. Ileal

578 enteroids were infected with PEDV-JMS or CV777 at an MOI of 5, and PEDV
579 production was determined at 24, 48, or 72 hpi by RT-qPCR (A) or viral titration (B).
580 (C). Representative images of ileal enteroids infected with PEDV-JMS or PEDV
581 CV777. Ileal enteroids were infected with PEDV-JMS or PEDV CV777 at an MOI of
582 5, and the level of PEDV infection was determined at 48 hpi by anti-PEDV N IFA.

583 **Fig. 6. PEDV infection suppresses the induction of innate IFN responses in ileal**
584 **enteroids.** (A and B). PEDV infection suppressed cellular IFN production at the early
585 stage of infection in ileal enteroids. The expression of IFN-α (A) or IFN-L1 (B) after
586 PEDV-JMS infection (MOI=5) was assessed by relative RT-qPCR. *, $P<0.05$, **,
587 $P<0.01$, ***, $P<0.005$, ****, $P<0.001$ vs. mock. (C). Inhibition of poly(I:C) elicited
588 IFN-L1 production by PEDV-JMS in enteroids. Ileal enteroids were infected with
589 PEDV-JMS at an MOI of 5 for 12 h and then stimulated with poly(I:C) for 12 h. Total
590 cellular RNA was purified, and the mRNA level of IFN-L1 was quantified by
591 RT-qPCR. The results are presented as the means ± SEMs (n=3).

592 **Fig. 7. IFN-L1 selectively induces a substantial IFN antiviral response and**
593 **inhibits PEDV infection in ileal enteroids compared with IFN-α.** (A-D). ISG
594 expression in ileal enteroids after IFN stimulation. Ileal enteroids were stimulated
595 with IFN at the indicated concentrations for 24 h, and the mRNA levels of ISG15 (A),
596 MxA (B), OASL (C), and IFITM1 (D) were quantified by RT-qPCR. (E-F). Inhibition
597 of PEDV infection in ileal enteroids by IFN-L1 and IFN-α. Intestinal enteroids were
598 primed with IFN for 24 h and infected with PEDV-JMS at an MOI of 1, and the
599 PEDV viral genome numbers (E) and titers (F) at 48 hpi were determined by

RT-qPCR and titration, respectively. The results are presented as the means ± SEMs (n=3).

References

1. **Peterson LW, Artis D.** 2014. Intestinal epithelial cells: regulators of barrier function and immune homeostasis. Nature reviews. Immunology **14:**141-153.
2. **Moon C, Stappenbeck TS.** 2012. Viral interactions with the host and microbiota in the intestine. Current opinion in immunology **24:**405-410.
3. **Sato T, van Es JH, Snippert HJ, Stange DE, Vries RG, van den Born M, Barker N, Shroyer NF, van de Wetering M, Clevers H.** 2011. Paneth cells constitute the niche for Lgr5 stem cells in intestinal crypts. Nature **469:**415-418.
4. **Sato T, Vries RG, Snippert HJ, van de Wetering M, Barker N, Stange DE, van Es JH, Abo A, Kujala P, Peters PJ, Clevers H.** 2009. Single Lgr5 stem cells build crypt-villus structures in vitro without a mesenchymal niche. Nature **459:**262-265.
5. **Kovbasnjuk O, Zachos NC, In J, Foulke-Abel J, Ettayebi K, Hyser JM, Broughman JR, Zeng XL, Middendorp S, de Jonge HR, Estes MK, Donowitz M.** 2013. Human enteroids: preclinical models of non-inflammatory diarrhea. Stem cell research & therapy **4 Suppl 1:**S3.
6. **Lanik WE, Mara MA, Mihi B, Coyne CB, Good M.** 2018. Stem Cell-Derived Models of Viral Infections in the Gastrointestinal Tract. Viruses **10**.
7. **Saxena K, Blutt SE, Ettayebi K, Zeng XL, Broughman JR, Crawford SE, Karandikar UC, Sastri NP, Conner ME, Opekun AR, Graham DY, Qureshi W, Sherman V, Foulke-Abel J, In J, Kovbasnjuk O, Zachos NC, Donowitz M, Estes MK.** 2016. Human Intestinal Enteroids: a New Model To Study Human Rotavirus Infection, Host Restriction, and Pathophysiology. Journal of virology **90:**43-56.
8. **Luu L, Matthews ZJ, Armstrong SD, Powell P, Wileman T, Wastling JM, Coombes JL.** 2018. Proteomic Profiling of Enteroid Cultures Skewed Towards Development of Specific Epithelial Lineages. Proteomics**:**e1800132.
9. **Barker N, Huch M, Kujala P, van de Wetering M, Snippert HJ, van Es JH, Sato T, Stange DE, Begthel H, van den Born M, Danenberg E, van den Brink S, Korving J, Abo A, Peters PJ, Wright N, Poulsom R, Clevers H.** 2010. Lgr5(+ve) stem cells drive self-renewal in the stomach and build long-lived gastric units in vitro. Cell stem cell **6:**25-36.
10. **Ettayebi K, Crawford SE, Murakami K, Broughman JR, Karandikar U, Tenge VR, Neill FH, Blutt SE, Zeng XL, Qu L, Kou B, Opekun AR, Burrin D, Graham DY, Ramani S, Atmar RL, Estes MK.** 2016. Replication of human noroviruses in stem cell-derived human enteroids. Science **353:**1387-1393.
11. **Ootani A, Li X, Sangiorgi E, Ho QT, Ueno H, Toda S, Sugihara H, Fujimoto K, Weissman IL, Capecchi MR, Kuo CJ.** 2009. Sustained in vitro intestinal epithelial culture within a Wnt-dependent stem cell niche. Nature medicine **15:**701-706.
12. **Lin CM, Saif LJ, Marthaler D, Wang Q.** 2016. Evolution, antigenicity and pathogenicity of global porcine epidemic diarrhea virus strains. Virus research **226:**20-39.
13. **Jung K, Saif LJ.** 2015. Porcine epidemic diarrhea virus infection: Etiology, epidemiology, pathogenesis and immunoprophylaxis. Veterinary journal **204:**134-143.
14. **Beall A, Yount B, Lin CM, Hou Y, Wang Q, Saif L, Baric R.** 2016. Characterization of a Pathogenic Full-Length cDNA Clone and Transmission Model for Porcine Epidemic Diarrhea Virus Strain PC22A. mBio **7:**e01451-01415.
15. **Jung K, Eyerly B, Annamalai T, Lu Z, Saif LJ.** 2015. Structural alteration of tight and adherens

junctions in villous and crypt epithelium of the small and large intestine of conventional nursing piglets infected with porcine epidemic diarrhea virus. Veterinary microbiology **177:**373-378.

16. **Zhang J, Guo L, Yang L, Xu J, Zhang L, Feng L, Chen H, Wang Y.** 2018. Metalloprotease ADAM17 regulates porcine epidemic diarrhea virus infection by modifying aminopeptidase N. Virology **517:**24-29.

17. **Zeng S, Zhang H, Ding Z, Luo R, An K, Liu L, Bi J, Chen H, Xiao S, Fang L.** 2015. Proteome analysis of porcine epidemic diarrhea virus (PEDV)-infected Vero cells. Proteomics **15:**1819-1828.

18. **Ji CM, Wang B, Zhou J, Huang YW.** 2018. Aminopeptidase-N-independent entry of porcine epidemic diarrhea virus into Vero or porcine small intestine epithelial cells. Virology **517:**16-23.

19. **Desmyter J, Melnick JL, Rawls WE.** 1968. Defectiveness of interferon production and of rubella virus interference in a line of African green monkey kidney cells (Vero). Journal of virology **2:**955-961.

20. **Koh SY, George S, Brozel V, Moxley R, Francis D, Kaushik RS.** 2008. Porcine intestinal epithelial cell lines as a new in vitro model for studying adherence and pathogenesis of enterotoxigenic Escherichia coli. Veterinary microbiology **130:**191-197.

21. **Zhang Q, Ke H, Blikslager A, Fujita T, Yoo D.** 2018. Type III Interferon Restriction by Porcine Epidemic Diarrhea Virus and the Role of Viral Protein nsp1 in IRF1 Signaling. Journal of virology **92**.

22. **Fu F, Li L, Shan L, Yang B, Shi H, Zhang J, Wang H, Feng L, Liu P.** 2017. A spike-specific whole-porcine antibody isolated from a porcine B cell that neutralizes both genogroup 1 and 2 PEDV strains. Veterinary microbiology **205:**99-105.

23. **van der Hee B, Loonen LMP, Taverne N, Taverne-Thiele JJ, Smidt H, Wells JM.** 2018. Optimized procedures for generating an enhanced, near physiological 2D culture system from porcine intestinal organoids. Stem cell research **28:**165-171.

24. **Thorne CA, Chen IW, Sanman LE, Cobb MH, Wu LF, Altschuler SJ.** 2018. Enteroid Monolayers Reveal an Autonomous WNT and BMP Circuit Controlling Intestinal Epithelial Growth and Organization. Developmental cell **44:**624-633 e624.

25. **Cheung R, Kelly J, Macleod RJ.** 2011. Regulation of villin by wnt5a/ror2 signaling in human intestinal cells. Frontiers in physiology **2:**58.

26. **Landry C, Huet C, Mangeat P, Sahuquet A, Louvard D, Crine P.** 1994. Comparative analysis of neutral endopeptidase (NEP) and villin gene expression during mouse embryogenesis and enterocyte maturation. Differentiation; research in biological diversity **56:**55-65.

27. **Jung K, Annamalai T, Lu Z, Saif LJ.** 2015. Comparative pathogenesis of US porcine epidemic diarrhea virus (PEDV) strain PC21A in conventional 9-day-old nursing piglets vs. 26-day-old weaned pigs. Veterinary microbiology **178:**31-40.

28. **Li L, Fu F, Xue M, Chen W, Liu J, Shi H, Chen J, Bu Z, Feng L, Liu P.** 2017. IFN-lambda preferably inhibits PEDV infection of porcine intestinal epithelial cells compared with IFN-alpha. Antiviral research **140:**76-82.

29. **Lin CM, Hou Y, Marthaler DG, Gao X, Liu X, Zheng L, Saif LJ, Wang Q.** 2017. Attenuation of an original US porcine epidemic diarrhea virus strain PC22A via serial cell culture passage. Veterinary microbiology **201:**62-71.

30. **Zhang J, Guo L, Xu Y, Yang L, Shi H, Feng L, Wang Y.** 2017. Characterization of porcine epidemic diarrhea virus infectivity in human embryonic kidney cells. Archives of virology **162:**2415-2419.

31. **Xue M, Zhao J, Ying L, Fu F, Li L, Ma Y, Shi H, Zhang J, Feng L, Liu P.** 2017. IL-22 suppresses the infection of porcine enteric coronaviruses and rotavirus by activating STAT3 signal pathway. Antiviral research **142:**68-75.

32. **Madson DM, Arruda PH, Magstadt DR, Burrough ER, Hoang H, Sun D, Bower LP, Bhandari M, Gauger PC, Stevenson GW, Wilberts BL, Wang C, Zhang J, Yoon KJ.** 2016. Characterization of Porcine Epidemic Diarrhea Virus Isolate US/Iowa/18984/2013 Infection in 1-Day-Old Cesarean-Derived Colostrum-Deprived Piglets. Veterinary pathology **53:**44-52.

33. **Darwich AS, Aslam U, Ashcroft DM, Rostami-Hodjegan A.** 2014. Meta-analysis of the turnover of intestinal epithelia in preclinical animal species and humans. Drug metabolism and disposition: the biological fate of chemicals **42:**2016-2022.

34. **Pelaseyed T, Bergstrom JH, Gustafsson JK, Ermund A, Birchenough GM, Schutte A, van der Post S, Svensson F, Rodriguez-Pineiro AM, Nystrom EE, Wising C, Johansson ME, Hansson GC.** 2014. The mucus and mucins of the goblet cells and enterocytes provide the first defense line of the gastrointestinal tract and interact with the immune system. Immunological reviews **260:**8-20.

35. **Johansson ME, Hansson GC.** 2016. Immunological aspects of intestinal mucus and mucins. Nature reviews. Immunology **16:**639-649.

36. **Wlodarska M, Thaiss CA, Nowarski R, Henao-Mejia J, Zhang JP, Brown EM, Frankel G, Levy M, Katz MN, Philbrick WM, Elinav E, Finlay BB, Flavell RA.** 2014. NLRP6 inflammasome orchestrates the colonic host-microbial interface by regulating goblet cell mucus secretion. Cell **156:**1045-1059.

37. **Johansson ME, Hansson GC.** 2014. Is the intestinal goblet cell a major immune cell? Cell host & microbe **15:**251-252.

38. **Jung K, Saif LJ.** 2017. Goblet cell depletion in small intestinal villous and crypt epithelium of conventional nursing and weaned pigs infected with porcine epidemic diarrhea virus. Research in veterinary science **110:**12-15.

39. **Schwegmann-Wessels C, Zimmer G, Schroder B, Breves G, Herrler G.** 2003. Binding of transmissible gastroenteritis coronavirus to brush border membrane sialoglycoproteins. Journal of virology **77:**11846-11848.

40. **Sun D, Shi H, Guo D, Chen J, Shi D, Zhu Q, Zhang X, Feng L.** 2015. Analysis of protein expression changes of the Vero E6 cells infected with classic PEDV strain CV777 by using quantitative proteomic technique. Journal of virological methods **218:**27-39.

41. **Hofmann M, Wyler R.** 1988. Propagation of the virus of porcine epidemic diarrhea in cell culture. Journal of clinical microbiology **26:**2235-2239.

42. **Schmittgen TD, Livak KJ.** 2008. Analyzing real-time PCR data by the comparative C(T) method. Nature protocols **3:**1101-1108.

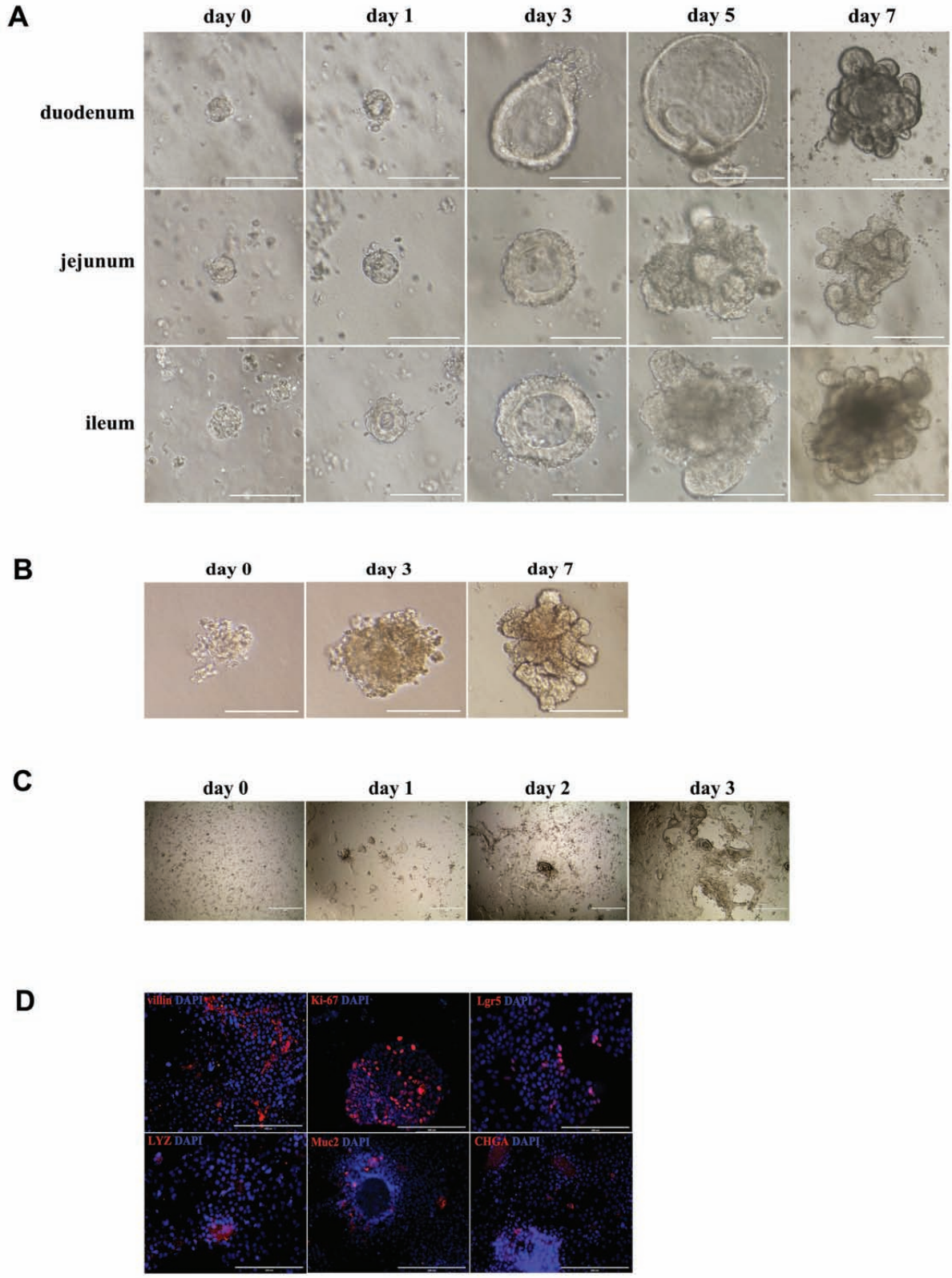

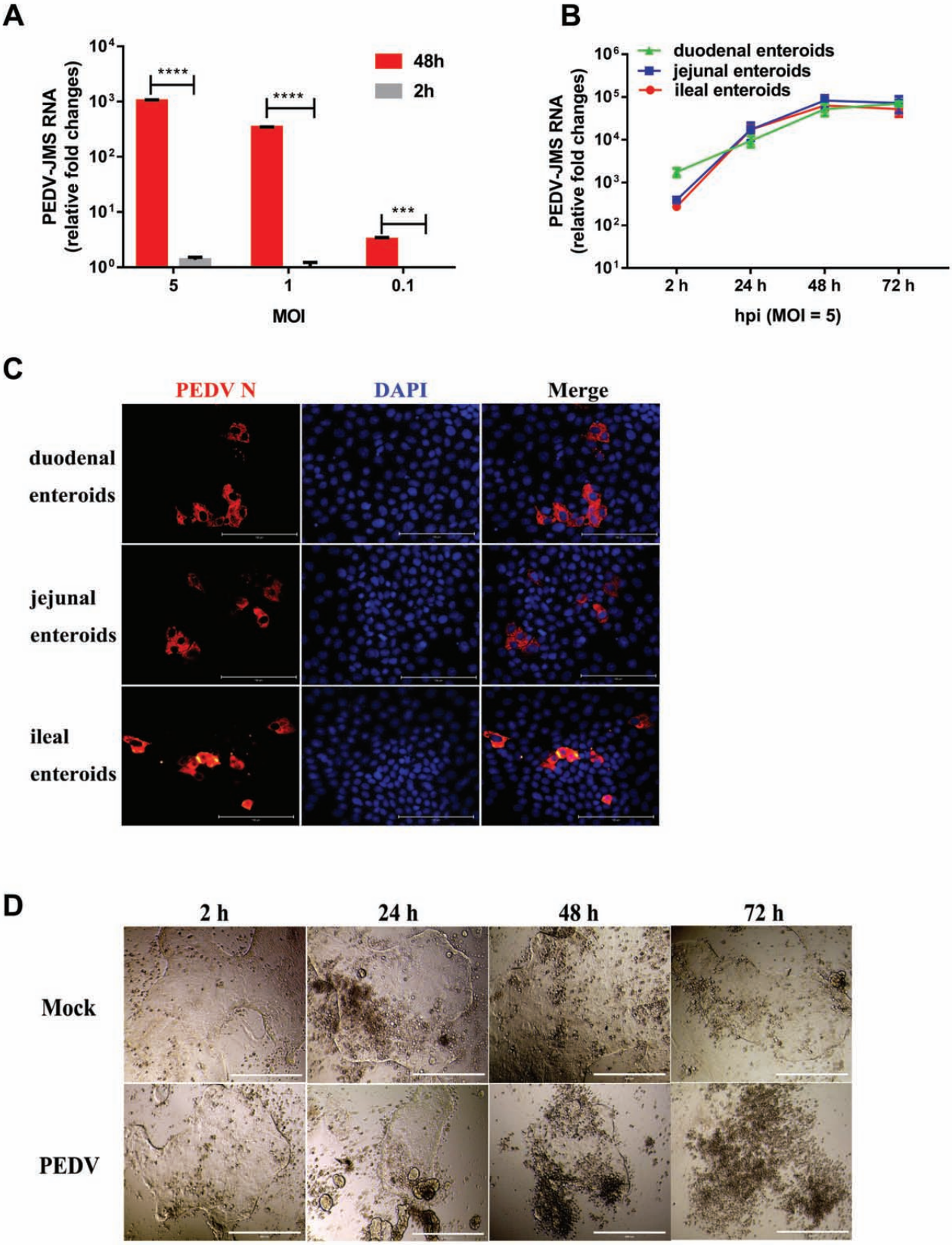

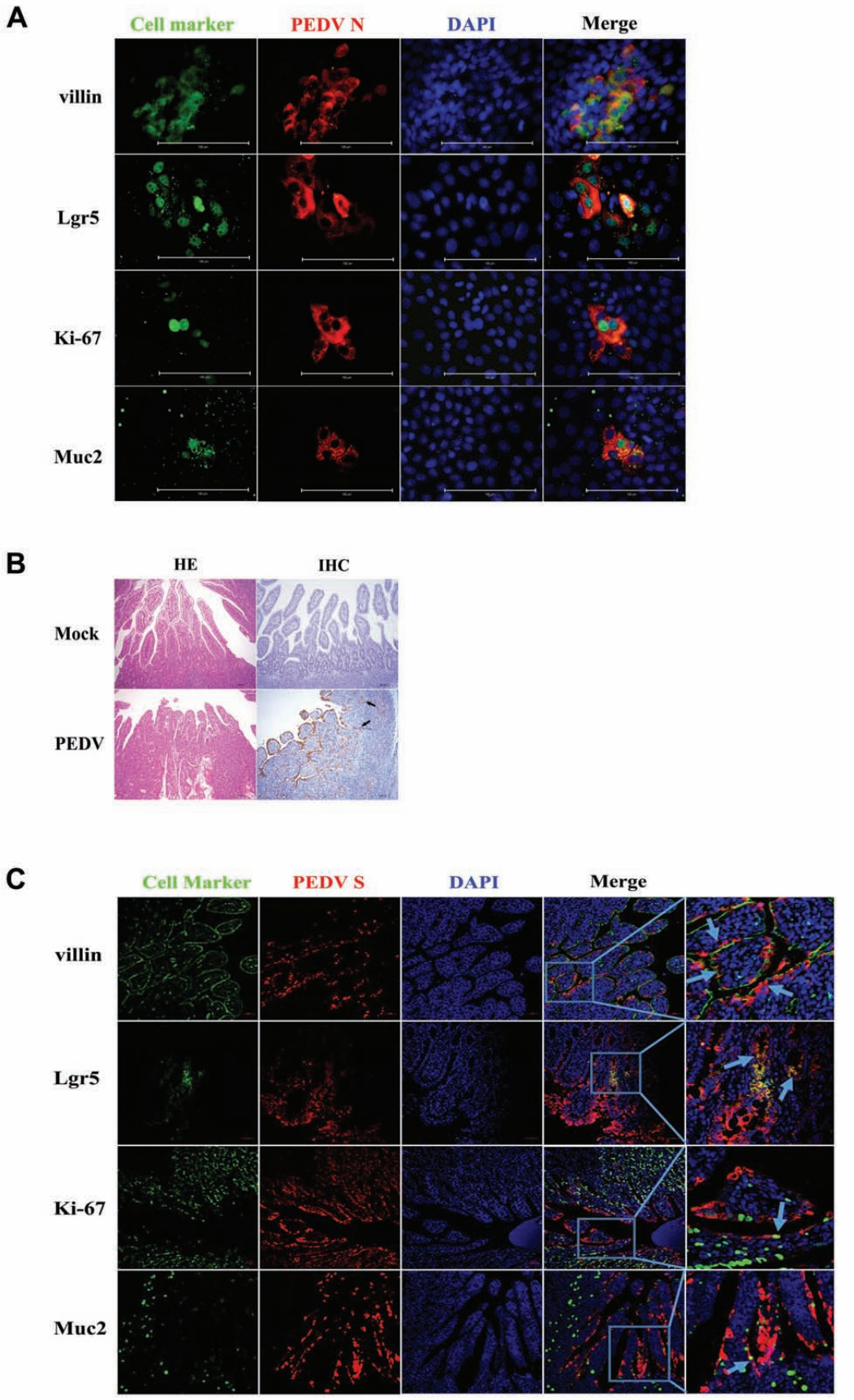

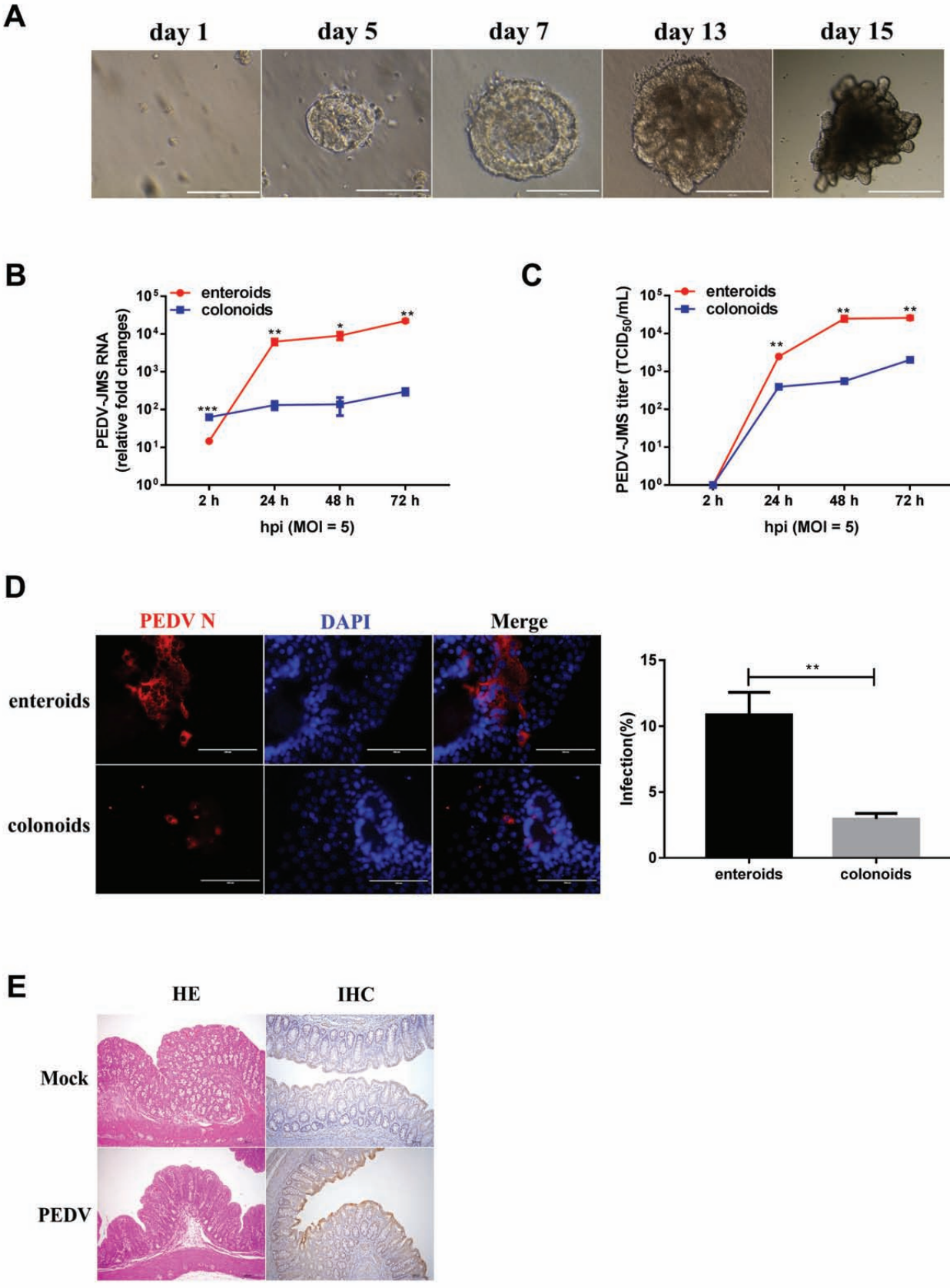

Journal of Virology